PHYSICAL CHARACTERIZATION OF FREEZE-DRIED FOAM PREPARED FROM *ALOE VERA* GEL AND GUAR GUM

CARACTERIZACIÓN DE ESPUMAS LIOFILIZADAS PREPARADAS A PARTIR DE GEL DE *Aloe vera* Y GOMA GUAR

Verónica SANTACRUZ-VÁZQUEZ[1*], Claudia SANTACRUZ-VÁZQUEZ[1], José Oscar LAGUNA CORTÉS[2]

ABSTRACT

Background: Foams are colloidal dispersions of a gas suspended in a dispersing phase, which consisting of a semi-freeze-dried or viscous liquid phase. The physical properties of food foams are the result of the bubble characteristics and their spatial arrangement. **Objectives:** The aim of this work was to obtain foams of *A. vera* gel and guar gum and describe the changes in their physical properties and microstructure during freeze-drying using the fractal dimension concept and image analysis techniques. **Methods:** The porosity, density, and volume expansion factor of the fresh foams that were based on the *A. vera* foams were determined. The kinetics of foam texture, color, porosity and microstructure of the freeze-dried foams were obtained. The fractal texture dimension of surface (FD_{SDBC}) and microstructure (FD_{ESEM}) of the foams were determined as indicators of structural changes after freeze-drying. The guar gum concentrations used to obtain the *A. vera* prefoam were expressed in w/w as F1 (control sample without gum), F2 (2%), F3 (4%) and F4 (6%). **Results:** We obtained stable freeze-dried foams of *Aloe vera* gel and guar gum. The porosity, density and volume expansion factor of the fresh and freeze-dried foams were affected by the addition of the guar gum. Changes in the topology of the freeze-dried foam surface during the drying process resulted in a high rugosity compared with the original smooth surface. The microstructure of the dried foam samples suggested a relationship between the gum concentration of the prefoam *A. vera* gel mixture and the physical properties before and after freeze-drying, such as an increase in the microstructural alterations and surface roughness during freeze-drying. The roughness of the freeze-dried foam surface, described by the FD_{SDBC} represented the macroscopic physical changes of the samples and correlated with the changes in the foam microstructure, which were described by the fractal dimension of the Environmental Scanning Electron Microscopy ESEM microphotographs (FD_{ESEM}). **Conclusions:** The digital analysis of the structure and porosity of the freeze-dried foam can be used to quantify the effect of gum concentrations on the morphological features and physical properties of foams during freeze-drying.

Keywords: Food property, foaming capacity, freeze-drying, *A. vera* gel foam, fractal analysis

---

[1] Benemérita Universidad Autónoma de Puebla, Facultad de Ingeniería Química, Ciudad Universitaria, 72570, Puebla, Pue., México.

[2] Instituto Tecnológico de Puebla, Av. Tecnológico No. 420. 72220, Puebla, Pue., México.

* Corresponding Author:: versanva@gmail.com

RESUMEN

Antecedentes: Las espumas son dispersiones coloidales de un gas en una fase líquida viscosa. Las propiedades físicas de las espumas alimentarias son el resultado de las características de sus burbujas y su disposición espacial. **Objetivos:** El objetivo de este trabajo fue obtener espumas de gel de *A. vera* y goma guar y describir los cambios en sus propiedades físicas y su microestructura durante el secado por liofilización utilizando el concepto de dimensión fractal y las técnicas de análisis de imagen. **Métodos:** Se determinó la porosidad, densidad, factor de expansión volumétrico de las espumas frescas de *A. vera*. Así como la cinética de liofilización, textura, isotermas de sorción, color, porosidad y la microestructura las espumas liofilizadas. La dimensión fractal de la textura (FD_{SDBC}) y microestructural (FD_{ESEM}) de las espumas de gel de *A. vera* y goma guar liofilizadas se determinó como un indicador de los cambios estructurales después de la liofilización. Las concentraciones de goma de guar utilizados para obtener la solución de clara de huevo preespuma se expresaron en w/w como F1 (muestra de control sin goma), F2 (2%), F3 (4%) y F4 (6%). **Resultados:** Fue posible obtener espumas liofilizadas estables de gel de *A. vera* y goma guar. La porosidad, densidad, factor de expansión volumétrico de las espumas se vieron afectadas con la adición de goma guar. Los cambios en la topología de la superficie de la espuma liofilizada durante todo el proceso de secado dieron lugar a alta rugosidad en comparación con la superficie lisa original. La microestructura de las muestras de espuma secas sugirió una relación entre la concentración de goma de las espumas de *A. vera* y las propiedades físicas antes y después de la liofilización como un aumento en las alteraciones microestructurales y rugosidad de la superficie durante el secado por congelación. La rugosidad de la superficie de la espuma liofilizada, se describió por la relación FD_{SDBC} que representa los cambios físicos macroscópicos de las muestras y se correlacionó con los cambios en la microestructura de espuma, que fueron descritos por la dimensión fractal de las micrografías ESEM (FD_{ESEM}). **Conclusiones:** El análisis digital de la estructura y la porosidad de la espuma liofilizada se puede utilizar para cuantificar el efecto de las concentraciones de goma guar en las características morfológicas de las espumas durante el secado por congelación.

Palabras clave: Propiedades de los alimentos, capacidad espumante, secado por liofilización, espumas de *A. vera*, análisis fractal.

INTRODUCTION

Foams are colloidal dispersions of a gas or gas mixture suspended in a viscous liquid phase (1). The physical properties of food foams (e.g., texture, density and stability) are the result of the bubble characteristics (e.g., size) and their spatial arrangement (2, 3). The most important factors contributing to the stabilization of foams and the avoidance of destabilization mechanisms are a high viscosity of the liquid phase and the presence of resistant and elastic adsorbed protein films (3). Commonly used stabilizers include natural hydrophilic and modified hydrophilic starches, gums, modified celluloses, pectin, gelatin and other proteins. Particularly, gums are often used to increase the viscosity of solutions and suspensions to form foams, and they act as thickeners in the aqueous dispersion phase. Gums may produce a particular texture, which is used to stabilize the dispersed phase or to reduce the formation of sugar or ice crystals in foams (4).

Aloe vera gel has wide applications in the cosmetic, nutraceutical and therapeutic industry. The gel of *A. vera* is used as an ingredient in cosmetics and medical products because its composition contains mannose polymers with sugars, including glucose and acemannan polymers, which are the active ingredients in the scar removal process. *A. vera* gel has vitamins, minerals, enzymes, proteins and phytosterol (5). This gel has therapeutic potential as an antidiabetic, anti-inflammatory, antioxidant, immunomodulatory, anti-ulcer, hepatoprotective, moisturizing agent, among other applications (6). However, thermal processing techniques affect the functionality of the chemical structures of *A. vera* gel, resulting in thermal damage and a denaturation process (7, 8). There are several treatments for the conservation of the gel, including convective drying and drum drying; however, these methods have disadvantages such as decreasing the antioxidant capacity of the gel when using a drying temperature of 50 to 90°C (9). Spray drying is another method

widely used to preserve Aloe extracts because it provides less damage to the biological activity of the final products compared with convective drying with forced air; this is due to the short processing times.

Moreover, the freeze-drying method has been extensively used in the pharmaceutical and food industries to obtain dehydrated materials that are easily degraded (10). Freeze-drying is often used because the process enables the retention of the physical and chemical properties of the products, such as the color, the vitamins, the antioxidant contents and other sensorial properties, including the original aroma and flavor. Here, freeze-drying was used for the dehydration of fresh *Aloe vera* foams (10, 11).

Guar gum is a galactomannan obtained from the endosperm of the Cyamopsis tetragonolobus seed. This polysaccharide is formed from galactose and mannose molecules and is used as a food additive in various foods products for stabilization. This additive is natural and economical. Its main property is to change in behavior of the water present in food. Guar gum swells and dissolves in polar solvents on dispersion and forms strong hydrogen bonds. The hydration rates are reduced in the presence of dissolved salts and other water-binding agents, such as sucrose (12).

The most significant characteristic of guar gum is its ability to form a viscous colloidal dispersion that is dependent on the time, temperature, concentration, pH and the time of agitation. However, guar gum was employed in this research because it is derived from a food instead of a bacterial exopolysaccharide, and it is not produced using common food allergens (13).

Recently, it was demonstrated that the microstructure of materials plays an important role in the physical properties of foodstuffs. Examples of these influences include the deformation and shrinkage that occurs during drying because microstructural characteristics of materials have an effect on the diffusion mechanisms and other parameters associated with moisture transfer (14). Kerdpiboon *et al.* (15) identified a relationship between the microstructural changes of carrot cubes and their physical alterations during air drying using fractal and image analysis. The concept of fractal texture was introduced to describe the rough or heterogeneous texture in the images and has been employed to quantify surface irregularity. According to Quevedo *et al.* (16), the texture of the images is usually called the texture feature (TF), and it is an important tool used in pattern recognition to characterize the arrangement of the basic constituents of a surface material. TF is useful in the analysis and description of natural scenes and environments and in the classification or categorization of pictorial data (17, 18). One method for determining texture features is the analysis of the surface intensity (SI), which is obtained by plotting the (x, y) pixel coordinates versus the gray level of each pixel (z axis) (19, 20). When the SI is characterized using the fractal dimension (FD), the TF is called the fractal texture of the image. If the FD is evaluated using the shifting differential box-counting method algorithm (SDBC), the FD is denoted as FD_{SDBC} (21). Furthermore, Pentland (22) showed that the fractal dimension of a surface dictates the fractal of the image intensity surface, which should be similar to the fractal dimension of the physical surface. Fractal texture has been reported to be sufficiently sensitive to allow for the detection of the surface roughness of products such as chocolate, bread, potatoes and other foods (23 - 27). The aim of this work was obtain foams of *A. vera* gel and guar gum and describe the changes in their physical properties and microstructure during freeze-drying using the fractal dimension concept and image analysis techniques.

MATERIALS AND METHODS

Selection and collection of the plants and the mucilage gel of the *A. vera* leaves

A. vera plants were collected from a herbarium of the Benemérita Universidad Autónoma de Puebla in Puebla, Mexico. The selected *A. vera* plants were 30 - 35 months-old with bright green leaves and without any visible spots. These plants had grown in controlled conditions in the herbarium in an area with partial shade and wide ventilation. The temperature inside the herbarium was 20±1°C. The specimens were planted with a spacing of approximately 0.50 m between plants. After cutting the leaves of the plants, they were washed with water to remove the dirt and dust to avoid contamination. Once the leaves were clean, we proceeded to separate the epidermis from the parenchyma fillet with a sterilized knife.

Preparation of the fresh foams

An ultrasonic homogenizer (UH-300, SMT, Japan) was used to disperse guar gum (Guarcel[R], México CAS no. 9000-30-0) in fresh *A. vera* gel (100 g) for 6 min at 20°C (1500 r min^{-1}). The guar gum concentrations used to obtain the prefoam solution of *A. vera* are expressed in w/w as F1 (control sample without gum), F2 (2%), F3 (4%) and F4 (6%).

Fresh foam density and volume expansion factor

The fresh foam density was determined by measuring the mass of a fixed volume of the foam. This determination was performed carefully to avoid destroying the foam structure and to ensure that there were no voids created while filling the foam into the measuring beaker. The density experiments were performed in triplicate (28).

To determine the physical structure of the four different foams, including the fresh *A. vera* gel without gum F1 (control sample), F2 (2%), F3 (4%) and F4 (6%), the foaming potential was measured with a volumetric procedure (28) using the following equation:

$$X = M/m \qquad (1)$$

where M is the mass of a strictly determined volume of the mixture prior to foaming (g), and m is the mass of the same volume of the mixture after foaming (g).

The foam volume expansion factor, Vo, was determined according to the following equation:

$$Vo = \frac{Vp}{V1} * 100 \ (\%) \qquad (2)$$

where Vp is the foam volume immediately after foam preparation (cm^3), and $V1$ denotes the volume of the solution (cm^3) used for foaming.

The porosity of the fresh foams was evaluated according to the following equation:

$$\varepsilon \ (\%) = \left(1 - \frac{\rho_p}{\rho_n}\right) * 100 \qquad (3)$$

where ρ_p is the density of the sample after bubble aeration, and ρ_n is the density of the sample prior to bubble aeration.

The foam stability factor was determined according to the following equation:

$$T = \left(\frac{A \ V}{A}\right) * 100 \ (\%) \qquad (4)$$

where A is the volume of the liquid from which the foam was made (cm^3), and V is the liquid leakage volume (cm^3) obtained during 15 min of foam storage.

Preparation of the freeze-dried foams

A similar procedure for preparation of the fresh foams was employed to obtain the freeze-dried foams. The prepared fresh foams were weighed, frozen and sublimated in a freeze-drying system Labconco 1 lt. (Labconco, Kansas City, MO, USA). Sample temperatures were reduced from 5 to −40°C at a constant cooling rate (−0.5 K min^{-1}), and the frozen samples were subsequently lyophilized at −20°C for 40 h. Then, the final weight and moisture content of the freeze-dried *A. vera* sample was measured (28). The moisture content (db) of the freeze-dried foams was evaluated according to AOAC method 32.1.03 (29). Each experimental freezing-drying run was conducted in triplicate, and the measurements of the corresponding physico-chemical properties of the *A. vera* foams were also repeated thrice.

Freeze-dried foam texture

A TAXT2 texture analyzer (Stable Micro Systems, Ltd., Godalming, Surrey, UK) was used to determine the firmness of the freeze-dried foams. The sample was placed on a hollow planar base (30), and a direct force was applied to the sample using a 5 mm spherical probe at a constant crosshead speed of 2 mm s^{-1}. A plot of the force *vs*. distance travelled by the plunger during the test was prepared. The hardness was defined as the maximum force in the force–deformation curve, and the crispness was characterized by the number of peaks and the slope of the first peak. Foam samples were tested, and the average values for hardness and crispness are reported (31).

Color measurement

A CIELAB colorimetry system was used to determine the foam colors using a WR10 8 mm Color Meter CIELAB (Graigar). The evaluated parameters, L (luminosity), a (red–green), and b (blue–yellow), were determined using the Hunter scale. Color was measured directly on the product surface. The total color difference (ΔE) was determined using the equation:

$$\Delta E = ((L_t - L_0)^2 + (a_t - a_0)^2 + (b_t - b_0)^2)^{1/2} \qquad (5)$$

where a_t is the Hunter scale coordinate indicating the redness or greenness of the foams at the final freeze-drying time, t, and a_0 is the same coordinate before the freeze-drying process, t = 0. The values, b_t and b_0, are the Hunter scale coordinates indicating the blueness or yellowness of the foams at the final freeze-drying time, t, and before the freeze-drying process at t = 0, respectively. L_t and L_0 re the Hunter scale coordinates indicating lightness of the foams at the final freeze-drying time, t, and before the freeze-drying process at t = 0, respectively, while ΔE is the total color difference (32).

Microstructure of the freeze-dried foams

The microstructure of the dried samples was examined using an Environmental scanning electronic microscope (ESEM) (LEO 1420VP, Carl Zeiss SMT AG, Oberkochen, Germany). Triplicate samples of the freeze-dried foam were viewed at 5000X magnification, and images were stored on a PC (AMD Turion X2, 500 GB, 500 MHz) as grayscale bitmaps with brightness values between 0 and 255.

Porosity of the freeze-dried foams

The image analysis software, ImageJ 1.34s (National Institutes of Health, NIH, USA), was used to quantify the characteristics of the porous freeze-dried foam, including the pore diameter and pore area. The image analysis was performed on the Image J software, and the algorithm used by this software was an automatic thresholding function, which is an iterative procedure based on the isodata algorithm (33). This algorithm divides the image into objects and background by taking an initial threshold. Then, the averages of the pixels at or below the threshold and pixels above are computed, and the averages of those two values are computed. The threshold is incremented, and the process is repeated until the threshold is larger than the composite average. There are many more methods for setting an automatic threshold, such as Otsu's method, entropy method, triangle method, k-means clustering, (33); however, in this study we used the cited algorithm because Image J was available for analysis of the image data.

Each pixel of an ESEM micrograph was assigned a gray intensity value (0 – 255). A threshold-based segmentation technique was employed to distinguish the pore from the freeze-dried phase using an appropriate gray level threshold. A binary image was then generated. The pixels with gray levels less than the selected threshold were assigned as pores and appeared black in a binary image, whereas the pixels with gray levels greater than the selected threshold were identified as the freeze-dried phase and appeared white in a binary image. Assuming a spherical shape, the pore diameter was estimated based on the known pore area. The pore area was determined by counting the number of pixels filled in the specified space (25).

Evaluation of the fractal texture dimension (FD_{SDBC}) of the freeze-dried foam surfaces

The lighting system used to obtain the images of the foam surfaces during freeze-drying included two lamps (15 V, 150 W, D 417053). A color digital camera Power Shot A620 digital camera (Canon Inc., Tokyo, Japan) was located vertically over the sample at a distance of 25cm and the angle between the camera axis and the light source was 45°. Considering that ambient illumination is very critical for reproducible imaging, the lighting system and the camera was put inside a wooden box whose internal walls were painted black to avoid the external light and reflections. The iris was operated in manual mode with a lens aperture of f = 8, speed setting of 1/6, and both zoom and flash were turned off to achieve repeatability.

Images were acquired of two sides of the foams, and were taken with no zoom, no flash, and a maximum resolution of the camera (2048*1536 pixels) and storage in JPEG format. *A. vera* foams images were acquired every 4 h during the drying period and they were saved on a PC (AMD Turion X2, 500 GB, 500 MHz) and then transformed from an RGB format to a black and white format as grayscale bitmaps. The brightness values were between 0 and 255 before calculating the fractal texture dimension (FD_{SDBC}).

The box-counting method was used to evaluate the fractal texture dimension (FD_{SDBC}) in the surface view images of the dried foams. In this study, the shifting differential box-counting method was employed to compute the fractal texture for the 2-D grayscale images of the foam surface. For this purpose, ImageJ 1.34s software (National Institute of Health, NIH, USA) and the codec proposed by Per Henden (Version 1.0, 2006-02-05) were used.

The fractal texture dimension (FD_{SDBC}) calculation was performed using an algorithm designed in MatlabTM Software (version 6.5) where FD_{SDBC0} and FD_{SDBC} are the fractal dimension texture of the foam surface images of the fresh sample and the sample at any given interval during freeze-drying, respectively.

A similar procedure was applied to obtain the evaluation of the fractal texture dimension in the ESEM microphotographs (FD_{ESEM}) of the freeze-dried foam. The microphotographs were saved on a PC (AMD Turion X2, 500 GB, 500 MHz) and then transformed from an RGB format to a black and white format as gray scale bitmaps. The brightness values ranged between 0 and 255 prior to calculating the fractal texture dimension (FD_{SDBC}), which was obtained by applying the previously mentioned procedure for the fractal texture dimension (FD_{SDBC}) of the freeze-dried foam surfaces (25).

All statistical analyses were performed using Minitab 13.1 software (Minitab Inc., Philadelphia State College, USA). A two-way analysis of variance ANOVA was applied to evaluate the effect of gum concentration in experimental data obtained from fractal texture of ESEM photomicrographs (FD_{ESEM}) and the fractal texture dimension (FD_{SDBC}) of the freeze-dried foam surfaces. Statistical analysis of Multiple Comparison Procedures were applied on the FD_{SDBC} values and FD_{ESEM} values using the Fisher LSD test to determine the presence of significant differences among FD_{SDBC} values and FD_{ESEM} values.

RESULTS

Fresh foam density

During the whipping process, air was brought into the *A. vera* gel prefoam and trapped in the liquid as bubbles. The foam density decreased as the whipping time increased, resulting in a minimum density after 3 min of whipping. As the concentration of gum increased in the F2, F3 and F4 samples, the foam density increased relative to foam F1. The initial foam density of approximately 0.93 g cm^{-3} decreased to 0.19, 0.26, 0.32 and 0.35 g cm^{-3} after 3 min of whipping for F1, F2, F3 and F4, respectively. After 5 min of whipping, an increase in the density was evident (0.27, 0.35, 0.60 and 0.68 g cm^{-3} for F1, F2, F3 and F4, respectively).

During the first 3 minutes of the whipping process, air was brought into the *Aloe vera* gel and entrapped in the liquid as bubbles (Fig 1). This led to a decrease in the foam density as the whipping time increased. The curves of the fresh *Aloe vera* gel foam densities during the whipping are similar to those of other foods that are high in viscosity, such as tomato paste foam (34). Beyond the five minutes, the foam density increased rapidly and was attributed to more thinning of the liquid film, more mechanical deformation and more bubble wall rupture during the extended whipping (31, 32). As the concentration of the guar gum increased to 2%, 4% and 6% (w/w), the foam density increased because the movement of the foaming agent from the aqueous phase towards the air–aqueous interface was limited and it was insufficient for the reduction in surface tension, which enhanced the foam formation (32).
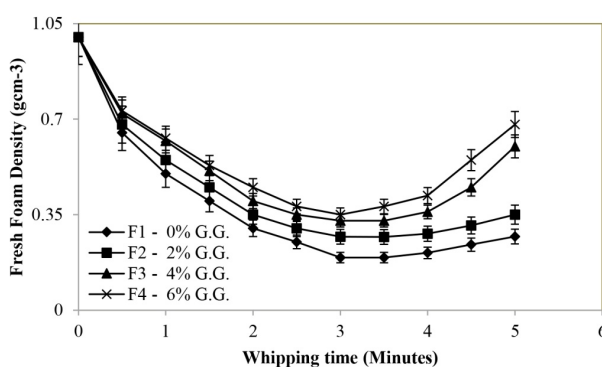

Figure 1. Fresh *A. vera* gel foam density as a function of the gum concentration during the whipping process

The gum concentration significantly affected the density of the fresh foams (ANOVA, $P<0.05$) based on the magnitudes of the F values (F=2.91). The results showed that the control sample (F1) exhibited the best foaming properties relative to the F2, F3 and F4 samples (Table 1). The samples with 4 and 6% guar gum concentrations in the *A. vera* gel foam showed much lower foaming parameters than F2, although the best results were obtained for the *A. vera* gel without gum (F1). This result indicates that the addition of guar gum substantially decreases the foaming potential of the *A. vera* gels. Similar results were obtained by Karim (30) using methyl cellulose in starfruit foams.

Porosity and mass density are important parameters of fresh foams. These two parameters are correlated because an increase in density is accompanied by a decrease in porosity. The foam with guar gum showed the lowest porosity (64.30% F4) and the highest density (0.35 g cm^{-3}) compared to products without gum.

Table 1. Comparison of the foaming potential of the fresh *A. vera* gel and the mixtures with guar gum.

	Foaming potential			
	Foam volume expansion factor Vo (%)	Foaming potential X	Foam Stability factor T (%)	Porosity (%)
Fresh Aloe vera gel, F1	162±2.5	1.18±0.03	43.00±2.8	78.22±2.4
Fresh Aloe vera gel with guar gum at 2% (w/w), F2	136.0±1.6	1.12±0.02	25.60±3.5	70.66±3.6
Fresh Aloe vera gel with guar gum at 4% (w/w), F3	118.0±1.8	1.11±0.02	17.80±2.4	65.46±2.8
Fresh Aloe vera gel with guar gum at 6% (w/w), F4	112.0±2.2	1.11±0.02	15.70±2.8	64.30±3.5

Kinetics of the freeze-dried foam under different drying conditions

The initial moisture content of the *A. vera* gel foams was 6.690.15 kg/kg db. The drying kinetics of F1, F2, F3 and F4 are presented in Fig. 2. The overall moisture content was reduced from 6.69, 5.32, 4.42 and 3.80 kg/kg db for F1, F2, F3 and F4, respectively, to 0.39 kg/kg db. Two different stages were observed in the freeze-drying curve of every tested formulation. The first stage extended over the first 20 h of drying (Fig. 2), the second stage also lasted 20 h, which corresponded to the equilibrium stage.
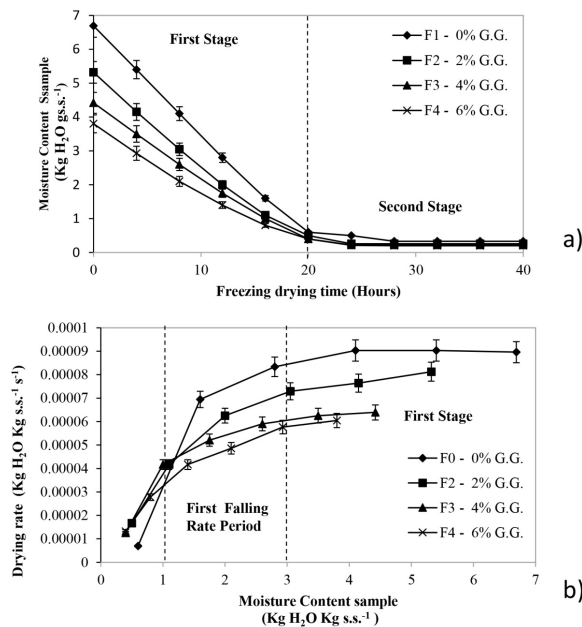

Figure 2. a) Moisture Content of *A. vera* gel foams. b) Drying rate of the *A. vera* gel foam during freeze-drying process.

A similar observation was reported by Lim *et al.* (35). The drying rate data that is presented in Fig. 2b shows a higher drying rate at the early stage of drying (first stage) because the moisture content of the *A. vera* gel foam decreased from the initial moisture content to approximately 3.0 kg/kg db.

The falling rate period could be divided into two periods according to the change in the drying rate curves. The first falling rate period (I) occurred between a moisture content of 3.0 and 1.0 kg/kg db, and it corresponded to the loss of free water. This water was freely available around the foam and could easily sublimate (36). The second rate period (II) exhibited a very low drying rate that decreased gradually with the decreasing moisture content, which was possibly due to the small amount of free water available given that the diffusion of bound water is the main mechanism controlling the water transport. In the last stage, the internal diffusion rate of moisture was found to decrease with time (Fig 2b).

Texture analysis of the freeze-dried foams.

The texture of the dried foams was evaluated using a compressive test (Fig. 3a). The maximum force of rupture is defined as the hardness, and the slope of the first peak was used to describe the crispness of the samples (37).
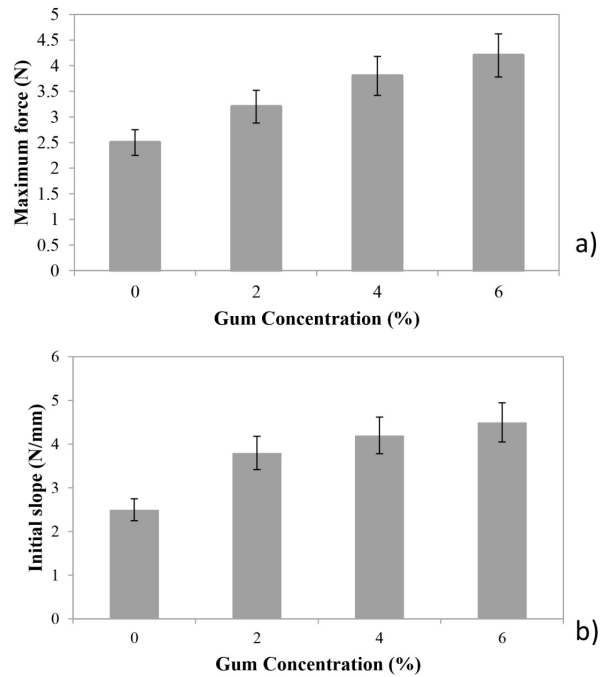

Figure 3. a) Maximum force of rupture. b) Initial slope of the first peak of dried *A. vera* gel foam with different gum concentrations.

The texture of the dried foams was strongly affected by the sample pore structure. F1 had a density of 0.19 g cm^{-3} and was characterized by larger pores and a limited number of smaller pores. F1 presented a lower density structure and lower strength values with respect to F2, F3 and F4. The maximum rupture forces of the samples were 2.52±0.23 N for F1, 3.28±0.22 N for F2, 3.80±0.40 N for F3 and 4.26±0.44 N for F4. The statistical analysis showed that the texture was significantly ($P<0.05$) affected by the gum concentration, as shown in Fig. 3a. Regarding the crispness, the F3 and F4 samples were spongy and were not crispy. These textural properties were similar to those reported for freeze-dried apple chips, which have a very porous structure (38). As shown in Fig. 3b, the gum concentration influenced the hardness and spongy textural features of the samples. Because the higher gum concentration in the fresh foam reduced the ability of water to act as a plasticizer in the dried foams, it caused a significant increase in the T_g and textural properties. This behavior was also observed for mango gel with maltodextrin, immature West Indian cherry with maltodextrin or gum Arabic and date palm with maltodextrin (36).

Color sample after freeze-drying

The total color difference, ΔE, of the *A. vera* foams before and after freeze-drying was obtained. The ΔE between the fresh *A. vera* foam and the freeze-dried samples were significantly different for F1 (ΔE=20), F2 (ΔE=25.5), F3 (ΔE=28.7) and F4 (ΔE=32.1). The color foams significantly changed with the freeze-drying process because the final dehydrated foams had a significantly lower luminosity than the fresh foam. The addition of the gum into the foam formulation produced a yellowish product whose intensity depended on the gum concentration.

Microstructure analysis of the freeze-dried foam tissue

Porosity measurement

The pore shapes of the *A. vera* gel foams before drying were spherical (not shown here). When the samples were freeze-dried, the pore shape changed. The pore size is shown in Fig. 4a.
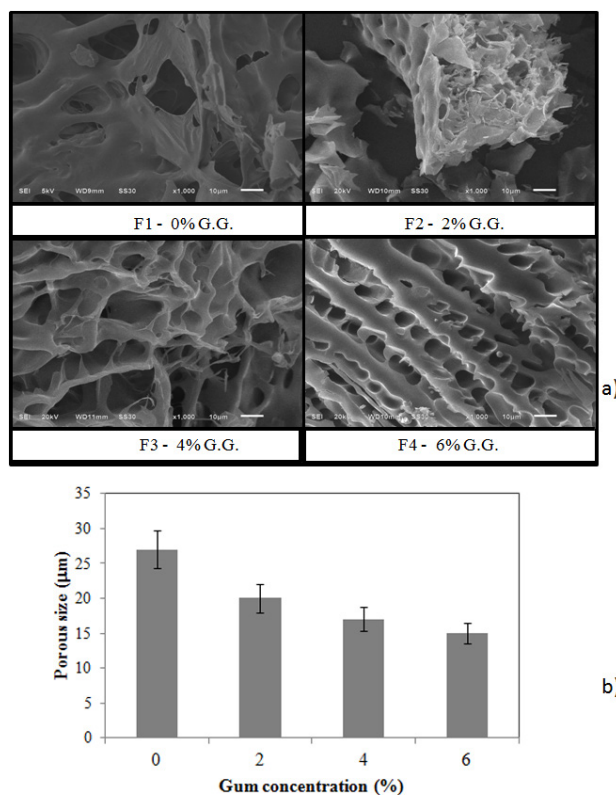

Figure 4. a) ESEM microphotographs and b) Pore size in the ESEM microphotographs of freeze-dried *A. vera* gel foams with different gum concentrations (1000X magnification, 20kV).

The pore diameter was estimated from the known pore area by assuming the spherical shape that was reported for F1. The foam density was found to affect the pore size of the *A. vera* gel foams. The F1 sample had an initial foam density of 0.19 g cm^{-3} and more large pores in the range of 15 - 20 μm than the samples with higher gum concentrations and higher foam densities. This large pore assembly might be generated by the coalescence of adjacent bubbles and the removal of ice crystals from the foam structure. However, the number of small pores that ranged from 5 – 10 μm was lower compared with the F3 and F4 samples. The pore size of foams F1, F2, F3 and F4 were 27±3.2, 20±2.5, 17±1.8 and 15±1.7μm, respectively. As shown in Fig. 4b, the F2 and F3 samples had few pores with diameters larger than 20 μm. The increases in the void area fraction of the samples during freeze-drying for F1, F2, F3 and F4 were 35.68, 33.06, 21.49 and 14.95%, respectively. As shown in Fig. 4a, the pore structure was significantly different among the samples with different gum concentrations.

The roughness of the freeze-dried foam microstructure (Fig. 5a), as described by the FD_{ESEM} values, represented the microscopic physical changes of the samples during the freeze-drying process. The foams without gum (F1) or with a low gum concentration (F2) exhibited higher FD_{ESEM} values than the other samples (Fig. 5).
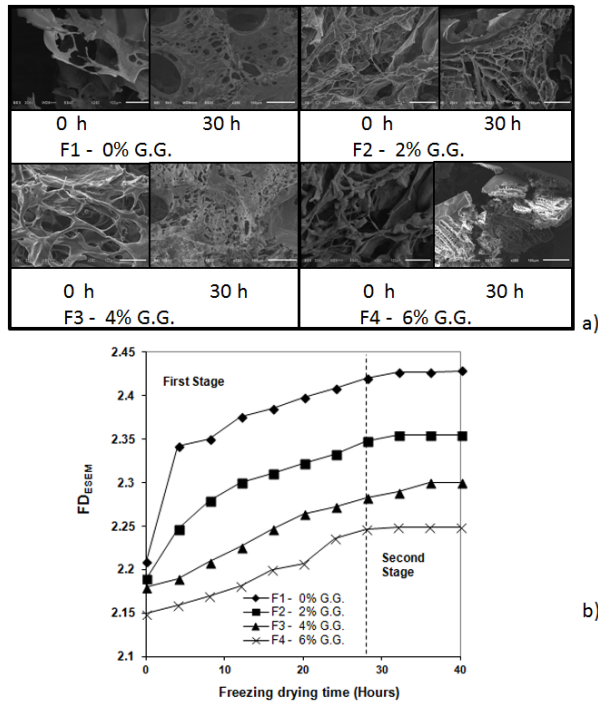

Figure 5. a) ESEM microphotographs of the freeze-dried foam (250X, 5kV) and b)FD_{ESEM} values of A. *vera* foams during freeze-drying at different gum concentrations

Under these conditions, the freeze-dried foam microstructure became rougher as a consequence of rapid water ice loss during freeze-drying, resulting in microstructural deformation of the pores. The maximum FD_{ESEM} values of the samples were 2.438 for F1, 2.361 for F2, 2.303 for F3 and 2.253 for F4. The multiple comparison analysis showed that the gum concentration in the foam formulations produced microstructural modifications with significant differences in the FD_{ESEM}.

The roughness of the freeze-dried foam surface (Fig. 6a), as described by the FD_{SDBC} values, represented the macroscopic physical changes of the samples and was correlated with changes in the freeze-dried foam texture and microstructure, which were described by the fractal dimension of the ESEM microphotographs(FD_{ESEM}).

Fig. 6b shows the variation of the FD_{SDBC} as a function of the freeze-drying time for the foams with different gum concentrations. The foam surface was mostly porous at the beginning of the freeze- drying with a FD_{SDBC} value of 2.220. However, during freeze-drying, the macroporous surface irregularity increased as a result of moisture loss, which was reflected by the increase in the FD_{SDBC}. Two different stages were observed in this curve. The first stage extended over the first 28 h of drying (Fig. 2) and exhibited a significant increase in the FD_{SDBC} compared to the second stage. The second stage lasted 12 h in which changes to the freeze-dried foam macroporous surface were less pronounced as the moisture content approached an equilibrium value (Fig. 6b).

The FD_{SDBC} values from the images of the dried freeze-dried foam were close to 2.24 to 2.35 during the last stage of drying, and neither further dehydration nor deformation occurred for the F1 formulation. Samples F3 and F4 exhibited a lower macroporous roughness and lower FD_{SDBC} values of the foam images (39).

Statistical analysis showed that the FD_{SDBC} value was significantly ($P<0.05$) affected by the gum concentration, as shown in Fig. 6b.
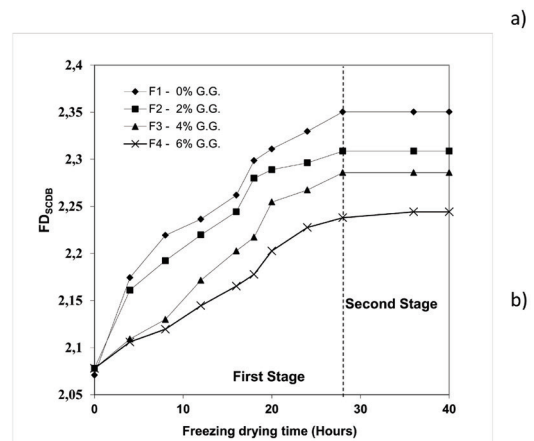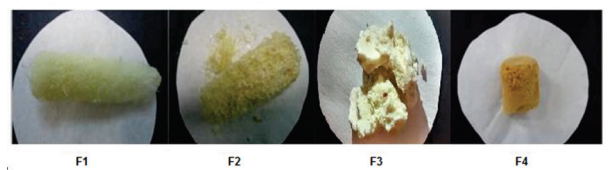

Figure 6. a) Images of the freeze-dried foam with different gum concentrations. b) FD_{SCDB} values of A. *vera* foams during freeze-drying at different gum concentrations.

DISCUSSION

The lowest density value for the F1 formulation was attributed to the fact that the movement of the foaming agent from the aqueous phase towards the air–aqueous interface was limited (30), and it was insufficient for a reduction in the surface tension, which enhances foam formation. As shown in Fig. 1, an increase in the gum concentration from 0.0% to 6.0% led to a greater than 50% increase in the foam density. The foam density curves during the whipping process presented a trend similar to those of other foods, such as tomato paste foam (30); i.e., the foams had a low density during the first 3 min, whereas there was an increase in the foam density at 5 min.

The drying rate data presented in Fig. 2b show that at the initiation of freeze-drying the sublimation front (moving boundary) is situated at the outer surface of the fresh foam sample.

During the freeze-drying process, the drying rates decreased with decreasing moisture content, signaling the beginning of the falling rate period (second stage). At this time, the sublimation front recedes from the outer surface of the foam towards the center of the sample resulting in an increased diffusion path for the sublimed moisture that was originated at the sublimation (ice) front; this renders an increased resistance to the internal diffusion of water vapor inside the sample (40, 41). The shape of the curves in Fig 2a and the drying rate in Fig 2b indicate that the internal diffusion of water vapor inside the sample is controlling the freeze-drying process. These results demonstrate the importance of the gum concentration on the moisture movement. The diffusion of water through the low-density foam was less constrained in the F1 formulation and decreased when the gum concentration in the *A. vera* gel foam increased in F2, F3 and F4.

The ESEM microphotographs showed that the freeze-dried foams exhibited a clearly deteriorated microstructure in which the removal of water ice was evident. At the high gum concentrations of F2, F3 and F4, dense products were obtained in the freeze-dried foam structure (Fig. 6a). F1 presented a more irregular microstructure pattern compared to the F2 and F3 foams in which the deformation of the structures was less pronounced. A heterogeneous foam structure was observed during freeze-drying in the absence of the gum.

The highest gum concentration (6%) produced the lowest irregularity in FD_{SDBC} and, consequently, the lowest FD_{SDBC} values. Under these conditions (F4), the deformation of the freeze-dried foam generated less roughness on the freeze-dried foam macroporous surface. At the intermediate gum concentrations, the deformation process was assisted by the high moisture transfer from the interior to the exterior of the freeze-dried foam. The kinetics of the variation of the deformation of the macroporous freeze-dried foam (FD_{SDBC}) was a function of the gum concentration and density, which also affected the overall quality of the final product. The freeze-dried foam without gum experienced a higher deformation, and the FD_{SDBC} values were higher than those obtained at higher gum concentrations.

The roughness of the freeze-dried foam surface, described by the FD_{SDBC} value, represented the macroscopic physical changes of the samples and correlated with changes in the foam microstructure, which were described by the fractal dimension of the ESEM microphotographs (FD_{ESEM}).

CONCLUSIONS

We obtained stable freeze-dried foams of *Aloe vera* gel and guar gum. The porosity, density and volume expansion factor of the fresh and freeze-dried foams were affected by the addition of guar gum. The microstructure of the dried foam samples suggested a relationship between the gum concentration in prefoam *A. vera* gel mixture and the physical properties before and after freeze-drying. Digital analysis of the structure and porosity of the freeze-dried foam was used to quantify the effect of gum concentrations on the morphological features of the foams during freeze-drying. The microstructure of the various samples suggested a relationship between the gum concentration and the density of the *A. vera* gel foams, which increased during freeze-drying. A simple relationship between the microstructural changes (FD_{ESEM}) of the freeze-dried foams and their gum concentration during freeze-drying was observed using combined fractal techniques and image analysis.

The addition of guar gum at concentrations of 2%, 4% and 6% produced high-density *Aloe vera* foams of 0.35, 0.60, and 0.68 $g\,cm^{-3}$, respectively, at an optimum whipping time of 3 min. The freeze-dried foams formed during the falling rate period with higher drying rates. An increased amount of

guar gum (6%) produced freeze-dried porous *Aloe vera* foams with increased amounts of hardness and crispness, low densities and smaller pore sizes. The analysis of the SEM microphotographs of the freeze-dried *Aloe vera* foams demonstrated that the addition of guar gum produced a pronounced a stable structure, which was also associated with the low values of the FD_{SDBC}. To produce a stable freeze-dried *Aloe vera* foam an addition of guar gum at 6% concentration is recommended.

ACKNOWLEDGMENTS

CONFLICT OF INTEREST

The authors declare that there is no conflict of interest with any financial organization regarding the material discussed in the manuscript.

ABBREVIATIONS

A = Volume of the liquid from which the foam was made (cm^3).

FD_{SDBC} = Fractal dimension texture of the foam surface images during the freeze-drying process.

D_{SDBC0} = Fractal dimension texture of the foam surface images prior to the freeze-drying process.

FD_{ESEM} = Fractal dimension texture of the freeze-dried foam determined from the ESEM photomicrographs.

FD_{ESEM0} = Fractal dimension texture of the fresh foam determined from the ESEM photomicrographs.

M = Mass of a strictly determined volume of the mixture before foaming (g).

m = Mass of the same volume of the mixture after foaming (g).

t = Freeze-drying time (min).

T = The foam stability factor.

V = Liquid leakage volume (cm^3) obtained during 15 min of foam storage.

$V1$ = Foam volume immediately after foam preparation (cm^3).

$V1$ = Foam volume of the solution (cm^3) used for foaming.

X= Foaming potential of the *A. vera* gel.

ε(%)= Porosity of the fresh foams.

ρ_p = Density of the sample after bubble aeration ($g\ cm^{-3}$).

ρ_n = Density of the sample before bubble aeration ($g\ cm^{-3}$).

REFERENCES

1. Prins, A. Advances in Food Emulsions and Foams, Dickinson E, Stainsby G. Eds. New York, U.S.A: Elsevier Applied Science; 1988. Principles of foam stability; 91-122.
2. Germain JC, Aguilera JM. Identifying industrial food foam structures by 2D surface image analysis and pattern recognition. J Food Eng. 2012 July; 111:440-448.
3. Sankat CK, Castaigne F. Foaming and drying behaviour of ripe bananas. LWT-Food Sci. Technol. 2004 August; 37: 517-525.
4. Mleko S, Kristinsson HG, Liang Y, Gustaw W. Rheological properties of foams generated from egg albumin after pH treatment. LWT-Food Sci. Technol. 2007 June; 40: 908-914.
5. Shabnam Javed, Atta-ur-Rahman. Chapter 9 – Alo vera Gel in Food, Health Products, and Cosmetics Industry. Stud. Nat. Prod. Chem. 2014, 41: 261-285.
6. Anirban RS, Dutta Gupta, Sampad Ghosh, Shashaank M, Aswatha Bibek Kabi. Chemometric studies on mineral distribution and microstructure analysis of freeze-dried *Aloe vera L*. gel at different harvesting regimens. Ind. Crop. Prod. 2013 November; 51: 194-201.
7. Cervantes-Martínez CV, Medina-Torres L, González-Laredo RF, Calderas F, Sánchez-Olivares G, Herrera-Valencia EE, Gallegos-Infante JA, Rocha-Guzman NE, Rodríguez-Ramírez J. Study of spray drying of the *Aloe vera* mucilage (*Aloe vera barbadensis miller*) as a function of its rheological properties. LWT-Food Sci. Technol. 2014 March; 55: 426-435.
8. Gulia A, Sharma HK, Sarkar BC, Upadhyay A, Shitandi A. Changes in physico-chemical and functional properties during convective drying of *Aloe vera* (Aloe *barbadensis*) leaves. Food Bioprod. Process. 2010 June; 88: 161-164.
9. Jafar F, Farid M. Analysis of Heat and Mass Transfer in Freeze-drying. Dry Technol. 2003 February; 21: 249 - 263.
10. Chakraborty R, Bera M, Mukhopadhyay P, Bhattacharya P. Prediction of optimal conditions of infrared assisted freeze-drying of *A. vera* (Aloe barbadensis) using response surface methodology. Sep. Purif. Technol. 2011 July; 80: 375-384.
11. Rey L, May JC. Freeze-Drying/ Lyophilization of Pharmaceutical and Biological Products. New York, U.S.A: Marcel Dekker Inc.; 2010. 580 pp.
12. Deepak M, Sheweta B, Bhupendar Singh K. Deep Guar gum: processing, properties and food applications—A Review. J Food Sci Technol. 2014 March; 51(3): 409-418.
13. Prabhanjan H, Gharia, MM, Srivastava HC. Guar gum derivatives. Part I:Preparation and properties. Carbohyd Polym. 1989 January; 11(4): 279–292.
14. Panyawong S, Devahastin S. Determination of deformation of a food product undergoing different drying methods and conditions via evolution of a shape factor. J. Food Eng. 2007 January; 78: 151-161.
15. Kerdpiboon S. Thesis Summary: Use of Fractal Analysis to Evaluate Physical Changes of Foods during Drying. Dry Technol. 2007 June; 25: 1131.
16. Quevedo R, López GR, Aguilera JM, Cadoche L. Description of food surfaces and microstructural changes using fractal image texture analysis. J. Food Eng. 2002 August; 53: 361-371.
17. Santacruz-Vázquez C, Santacruz-Vázquez V, Chanona-Perez J, Jaramillo-Flores M E, Welti-Chanes J, Gutierrez-Lopez G F. Encyclopedia of Agricultural, Food, and Biological Engineering, 2nd ed. Boca Raton, Florida U.S.A: CRC Press; 2010 Oct 21. Fractal Theory Applied to Food Science; 1-12 p.

18. Santacruz-Vázquez V, Santacruz Vázquez C, Laguna-Cortés JO, Toxqui-López S. Cambios en la textura de la superficie de esferas de melón (Cucumis melo cantalupensis) durante el secado por fluidización. Vitae. 2013 November; 20(3): 161-171.

19. Valous NA, Drakakis K, Sun DW. Detecting fractal power-law long-range dependence in pre-cooked pork ham surface intensity patterns using Detrended Fluctuation Analysis. Meat Sci. 2010 October; 86(2): 289 - 297.

20. Valous NA, Mendoza F, Sun DW, Allen P. Texture appearance characterization of pre-pork ham images using fractal metrics: Fourier analysis dimension and lacunarity. Food Res. Int. 2009 April; 42: 353 - 362.

21. Wen-Shiung Ch, Shang-Yuan Y, Chih-Ming H. Two algorithms to estimate fractal dimension of gray-level images. Opt. Eng. 2003 August; 42(8): 2452 – 2464.

22. Pentland AP. Fractal based description of natural scenes. IEEE T Pattern Anal. 1984 November; 6: 661- 674.

23. Kerdpiboon S, Devahastin S, Kerr WL. Comparative fractal characterization of physical changes of different food products during drying. J. Food Eng. 2007 December; 83: 570 -580.

24. Dàvila E, Parés D. Structure of heat-induced plasma protein gels studied by fractal and lacunarity analysis. Food Hydrocolloid. 2007 March; 21: 147 – 153.

25. Kerdpiboon S, Kerr WL, Devahastin S. Neural network prediction of physical property changes of dried carrot as a function of fractal dimension and moisture content. Food Res. Int. 2006 December; 39: 1110 - 1118.

26. Pedreschi F, Aguilera JM, Brown CA. Characterization of food surfaces using scale-sensitive fractal analysis. J. Food Process. Eng. 2000 January; 23: 127-143.

27. Xu P, Mujumdar AS, Yu B. Fractal Theory on Drying: A Review. Dry Technol. 2008 May; 26: 640-650.

28. Thuwapanichayanan R, Prachayawarakorn S, Soponronnarit S. Drying characteristics and quality of banana foam mat. J. Food Eng. 2008 June; 86: 573 -583.

29. Association of Official Analytical Chemists International, AOAC. Official methods of analysis; 16th Ed.; Arlington, Virginia, USA, 1995.

30. Karim AA, Wai CC. Characteristics of foam prepared from starfruit (Averrhoa carambola L.) puree by using methyl cellulose. Food Hydrocolloid. 1999 May; 13: 203 -210.

31. Haihong Zhang, Guiying Xu, Teng Liu, Long Xu, Yawen Zhou. Foam and interfacial properties of Tween 20- bovine serum albumin systems. Colloid surface A. 2013 January; 416: 23-31.

32. Karim AA, Wai CC. Foam-mat drying of starfruit (*Averrhoa carambola L.*) puree. Stability and air drying characteristics. Food Chem. 1999 February; 64: 337-343.

33. Ridler TW, Calvard S. Picture thresholding using an iterative selection method, IEEE T Syst Man CY C, SMC-8 1978: 630- 632.

34. Cooke RD, Breag GR, Ferbe CEM, Best PR, Jones J. Studies of mango processing I. The foam-mat drying of mango (Alphonso cultivar) puree. Int. J. Food Sci. Tech. 1976 October; 11: 463- 473.

35. Lim LT, Tang J, He J. Moisture sorption characteristics of freeze-dried blueberries. J. Food Sci. 1995 July; 60: 810 -814.

36. Hamdami N, Monteau JY, Le Bail A. Transport properties of a high porosity model food at above and sub-freezing temperatures. Part 2: Evaluation of the effective moisture diffusivity from drying data. J. Food Eng. 2004 May; 62: 385 – 392.

37. Vickers Z, Bourne MC. Crispness in food -A review. J. Food Sci. 1976, 41: 1153 -1157.

38. Sham PWY. Scaman CH, Durance TD. Texture of vacuum dehydrated apple chips as affected by calcium pretreatment, vacuum level, and apple variety. J. Food Sci. 2001 November; 66: 1341 -1347.

39. Santacruz-Vázquez C, Santacruz-Vázquez V. The spatial distribution of ß-carotene impregnated in apple slices determined using image and fractal analysis. J. Food Sci. Tech. 2013 July. Doi 10.1007/s13197-013-1097-5.

40. Rahman MS, Al-Amri OS, Al-Bulushi IM. Pores and physico-chemical characteristics of dried tuna produced by different methods of drying. J. Food Eng. 2002 August, 53: 301-313.

41. Rahman MS, Toward prediction of porosity in foods during drying: A brief review. Dry Technol. 2001, 19: 1-13.